Sensor applications

Enhancing Surgical Laparoscopic Video Quality Assessment With Integrated Feature Fusion Accounting for Sensor and Transmission Distortions

Ajay Kumar Reddy Poreddy[1], Priyanka Kokil[2]*, and Balasubramanyam Appina[3]*

[1]*Department of Computer Science, Engineering, Sri Sivasubramaniya Nadar College of Engineering, Chennai 603110, India*
[2]*Advanced Signal and Image Processing (ASIP) Lab., Department of Electronics, Communication Engineering, Indian Institute of Information Technology, Design, Manufacturing, Kancheepuram, Chennai 600127, India*
[3]*Multimedia Engineering and Perceptual Cognitive Analysis Group (MEPCAG), Indian Institute of Technology Indore, Indore 453552, India*
**Senior Member, IEEE*

Manuscript received 5 November 2024; revised 11 March 2025; accepted 17 March 2025. Date of publication 20 March 2025; date of current version 21 April 2025.

Abstract—In this letter, an opinion-aware quality assessment (QA) model for surgical laparoscopic videos (LVs) considering sensor and transmission distortions is proposed based on statistical disparities between luminance and color components of the opponent color space (OCS). First, the luminance variations among the frames of distorted LVs are computed based on the energy of the Gabor subbands and weighted histogram features of the local binary pattern map. Second, the color degradations of each frame of LV are estimated based on the chromatic components of the OCS using moment statistics and the shape and spread parameters of the asymmetric generalized Gaussian distribution. These features are computed across two scales, concatenated, and pooled to obtain the overall quality representative feature set of the LVs. Finally, an AdaBoost back propagation neural network is utilized to map the extracted feature set to quality scores using labels as surgeons opinion scores. Extensive experiments demarcate that the proposed QA model for surgical LVs outperforms the existing video QA models with an overall linear correlation coefficient of 0.9800 and Spearman rank order correlation of 0.9247 on the LVQA dataset, respectively.

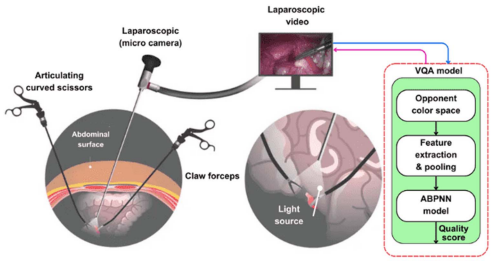

Index Terms—Sensor applications, Gabor subbands, laparoscopic videos (LV), local binary pattern, opponent color space (OCS).

I. INTRODUCTION

The global laparoscopic device and accessories market surpassed $10.9 billion in 2020 and is projected to near $15.8 billion in 2026 with a 3.2% growth rate, driven by the increasing adoption of minimally invasive techniques [1]. With over 13 million laparoscopic procedures performed annually worldwide, this approach, facilitated by small incisions, offers efficient access to the abdomen and pelvis, transforming surgical practices [2]. Through small incisions, a light source and a laparoscopic imaging sensor are inserted, and surgical operations are performed with the instruments while the imaging sensor transmits visual data to a monitor, providing real-time data to the surgeon. However, imaging sensor movements during surgery introduce several distortions, such as motion blur, uneven illumination, and defocus blur, which degrades the quality of laparoscopic videos (LV). These distortions pose challenges to surgical decision making and may compromise the overall performance of the surgical procedure. Consequently, there arises a need to analyze and evaluate LV quality to optimize surgical efficiency.

Quality assessment (QA) of LVs is categorized into subjective and objective. In subjective assessment, surgeons rate the quality of the LVs displayed on the monitor. These ratings are then averaged and normalized to estimate the mean opinion score (MOS) of the LVs. However, calculating the MOS is expensive and labor-intensive due to the surgeons involvement. Despite this, the scores obtained from subjective assessments are crucial for evaluating objective algorithms [3]. On the other hand, objective QA methods automatically predict the quality of LV based on an algorithm and are classified into three categories: Full-Reference (FR), Reduced-Reference (RR), and No-Reference (NR). FR QA algorithms require complete knowledge of the pristine LV, and RR QA algorithms require ancillary features of the pristine LV. In contrast, NR QA algorithms do not need pristine LV to assess the quality of the test LV.

Over the years, few QA models [4], [5], [6], [7] have been proposed to improve the perceptual quality of LVs. In [8], the authors modeled the spectral and correlation-based measurements between reference and distorted LVs using various perceptual distance metrics. Biswas and Palanisamy [9] utilized a fuzzy network and a bivariate generalized Gaussian distribution (BGGD) model to compute the quality of distorted motion blur LVs. In [10], the perceptual variations of unevenly illuminated surgical LVs are computed by averaging the discrepancies between distorted and contrast-enhanced components of LV frames. Khan et al. [11] proposed a QA model for surgical LVs with stacked ResNet-18 networks that can identify distortion type and the quality discrimination of test LVs. In our prior work [12], the structural variations of LV frames are computed based on eigenanalysis of the singular value decomposition (SVD). Further, the aggregated features computed from eigen matrices of SVD are fed to a trained support vector regressor (SVR) to estimate the LV quality.

When LVs are affected by distortions such as Gaussian noise, defocus blur, motion blur, smoke, and uneven illumination, the luminance, texture, and color properties of the LVs are significantly altered. Gaussian noise adds grainy artefacts that obscure textures, defocus and motion blur, reduce sharpness and contrast, smoke lowers

Corresponding author: Priyanka Kokil (e-mail: kokilnit@gmail.com).
Associate Editor: Francisco Falcone.
Digital Object Identifier 10.1109/LSENS.2025.3553292

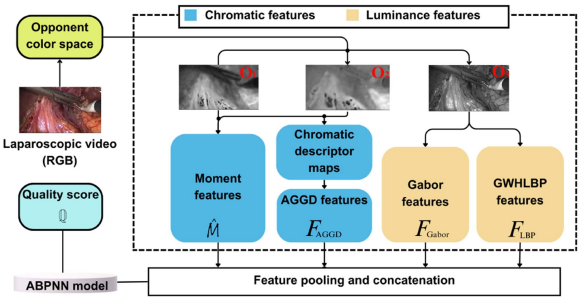

Fig. 1. Framework for predicting quality score of a test surgical LV.

luminance and desaturates colors, and uneven illumination creates nonuniform brightness, causing overexposure, underexposure, and color shifts. These distortions degrade visual quality, affecting surgical decision-making and may compromise the overall performance of the surgical procedure. To the best of our knowledge, existing literature [8], [9], [10], [11], [12] primarily focus on capturing spatial and structural variations, while often overlooking important perceptual attributes such as luminance, texture and color, which are crucial for accurately assessing the visual quality from a surgeons perspective. This gap highlights the need for improvement in assessing the quality of LVs, particularly where current QA models fail to address LV specific distortions, providing motivation for our QA model. Therefore, an NR QA model for surgical LVs is proposed by considering the aforementioned components of LVs with key contributions outlined as follows.

1) An opinion-aware QA model for surgical LVs is proposed based on spatial and color components of opponent color space (OCS).
2) The spatial discriminations of LVs are computed based on the Gabor subbands and the histogram features of a gradient-weighted histogram of the local binary pattern (GWHLBP).
3) The color variations of LVs are estimated based on five chromatic maps developed based on two color components of the OCS.
4) The computed feature sets and surgeons opinion scores are given to the AdaBoost back propagation neural network (ABPNN) to estimate the quality of test LV.

The rest of this letter is organized as follows. Section II introduces the proposed QA model. Section III outlines the results. Finally, Section IV concludes this letter.

II. METHODOLOGY

We propose an LVQA model based on the perceptual representations of the LV computed using spatial and color characteristics of the human visual system (HVS). First, each frame of LV is transformed to OCS, and the quality representative features are modeled based on the statistics of the Gabor energy, GWHLBP, and natural scene statistics (NSS). Then, these quality-aware features are averaged over the number of LV frames and given to the ABPNN to estimate the perceptual deviation of the distorted LV. The framework for predicting the quality score of a test surgical LV is shown in Fig. 1.

A. Feature Extraction

1) Color Space Conversion: Due to high correlation among the RGB color channels, many works [7], [10] converted RGB color space to OCS as it better represents the HVS. Motivated by [7], [10], we convert each frame of LV to OCS as follows:

$$\begin{bmatrix} O_1 \\ O_2 \\ O_3 \end{bmatrix} = \begin{bmatrix} \frac{1}{\sqrt{2}} & \frac{-1}{\sqrt{2}} & 0 \\ \frac{1}{\sqrt{6}} & \frac{1}{\sqrt{6}} & \frac{-2}{\sqrt{6}} \\ \frac{1}{\sqrt{3}} & \frac{1}{\sqrt{3}} & \frac{1}{\sqrt{3}} \end{bmatrix} \begin{bmatrix} R \\ G \\ B \end{bmatrix} \tag{1}$$

where O_1, O_2 are chromatic components and O_3 is the luminance component.

2) Statistics of Luminance Component: In order to measure the statistical perturbations caused by the O_3 component, the luminance features are modeled based on Gabor decomposed subbands and the LBP map.

a) Gabor features: Cortical neurons in the V1 area of the visual cortex decompose the visual data into different spatial components using different orientation filters, whose responses are squared and combined over multiple phases to capture the bandpass responses of the HVS. Here, we utilize a 2-D Gabor filter, as it represents a better approximation for V1 responses of the HVS [13]. Further, the O_3 component of each frame of LV is convolved with the Gabor filter across two scales ($q \in \{1, 2\}$) and six orientations ($\theta \in \{0°, 30°, 60°, 90°, 120°, 150°\}$) and the energy of the Gabor subbands ($E_g^{q\theta}$) is computed to estimate the frame level Gabor feature set of the LV. Subsequently, these features are averaged over the number of frames ($n = 1, 2, \ldots, \tau$; τ = total number of frames) to estimate the overall Gabor feature representation (F_{Gabor}) of the LV. Since, the Gabor features are extracted at two scales and six orientations, the cardinality of (F_{Gabor}) is 1×12

$$F_{\text{Gabor}} = \frac{1}{\tau} \sum_{n=1}^{\tau} E_{gn}^{q\theta}. \tag{2}$$

b) GWHLBP features: The HVS is highly sensitive to local texture variations, which are crucial for distinguishing between different tissue types and detecting fine structures in LVs [14]. Motivated by [14], textural features are calculated using the LBP map. Initially, the O_3 component of each frame of LV undergoes gradient mapping via the Prewitt operator. Further, LBP is applied on the gradient map with radius one and eight neighbors to encode primitive structures, including lines, points, and edges, forming the gradient LBP (GLBP) map. Finally, the gradient-weighted LBP features are computed using a histogram (H_{GLBP}) by assigning weights (Φ) to the pixels ($i = 1, 2, \ldots T$; T = total number of pixels in each LV frame) that share the common GLBP pattern as follows:

$$H_{\text{GLBP}}(p) = \sum_{i=1}^{T} \Phi_i \mathcal{L}(\text{GLBP}(i), p) \tag{3}$$

$$\mathcal{L}(m, n) = \begin{cases} 1, & \text{if } m = n \\ 0, & \text{otherwise} \end{cases} \tag{4}$$

where $p \in [0, P]$ is the possible combinations in the GLBP map with a similar pattern, P = total number of possible combinations. Subsequently, the $H_{\text{GLBP}}(p)$ features are computed across two scales and averaged over the total frames to estimate the overall texture feature representation (F_{LBP}) of the LV.

$$F_{\text{LBP}} = \frac{1}{\tau} \sum_{n=1}^{\tau} H_{\text{GLBP}_n}^{q}. \tag{5}$$

It is important to note that the F_{LBP} features are computed across two scales only as the LBP map is rotational invariant. The cardinality of F_{LBP} is 1×20.

3) Statistics of Color Components: In order to measure the perceptual degradations caused by color changes in LVs, our proposed model computes five chromatic descriptor maps based on O_1, O_2 components of the OCS. These maps measure the perceptual chromatic deviations in diverse perspectives, and then the quality discernible parameters of LVs are estimated based on the statistics of the empirical histograms of five color descriptor maps. These maps include absolute difference map (D), saturation map (S), angle component (A), and two angle derivation opponent maps (A_x, A_y)

$$D = |O_1 - O_2|, \qquad S = \sqrt{O_1^2 + O_2^2}$$

$$A = \arctan\left(\frac{O_1}{O_2 + \epsilon}\right), A_x = \arctan\left(\frac{\Delta_x}{\Delta_y + \epsilon}\right)$$

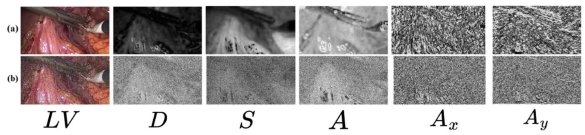

Fig. 2. Illustration of five chromatic attributes computed from two color components of the OCS from 100th frame of 'video10' of the LVQA dataset. (a) Reference maps. (b). Distorted maps.

$$A_y = \arctan\left(\frac{\Delta_y}{\Delta_x + \epsilon}\right) \tag{6}$$

where Δ_x and Δ_y are partial Gaussian derivative gradient maps computed along horizontal and vertical directions, respectively, and ϵ (> 0) is a constant to avoid the instability caused due to division by zero. Fig. 2 visualizes the five chromatic maps (D, S, A, A_x, A_y) of 100th frame of reference and distorted LV named "video 10" of the LVQA dataset. The figure clearly demonstrates that these chromatic maps are perturbed with Gaussian noise stimuli compared to reference stimuli. Further, these maps are processed via mean subtracted coefficient normalization (MSCN) operation [7] to reduce the variations among the neighborhood pixels. Fig. 3 depicts the empirical histograms of (D, S, A, A_x, A_y) of 100th frame of reference and various distorted versions of LV named "video 10" of the LVQA dataset after performing MSCN operation. The histograms of (D, S, A, A_x, A_y) exhibited asymmetrical Gaussian distributions with zero mean. Also, it is important to observe that for each chromatic map, the empirical histogram shapes are different, implying the scale (γ_l, γ_r) and shape (δ) parameter of AGGD can be utilized to model the chromatic descriptor maps of surgical LVs. The AGGD model of a row vectorised feature vector (Z) is given as

$$\mathbb{P}(Z; \delta, \gamma_l^2, \gamma_r^2) = \begin{cases} \frac{\delta}{(\vartheta_l+\vartheta_r)\Gamma\left(\frac{1}{\delta}\right)} \exp\left(-\left(-\frac{Z}{\vartheta_l}\right)^{\delta}\right); Z < 0 \\ \frac{\delta}{(\vartheta_l+\vartheta_r)\Gamma\left(\frac{1}{\delta}\right)} \exp\left(-\left(\frac{Z}{\vartheta_l}\right)^{\delta}\right); Z \geq 0 \end{cases} \tag{7}$$

where

$$\vartheta_l = \gamma_l \sqrt{\frac{\Gamma\left(\frac{1}{\delta}\right)}{\Gamma\left(\frac{3}{\delta}\right)}}, \vartheta_r = \gamma_r \sqrt{\frac{\Gamma\left(\frac{1}{\delta}\right)}{\Gamma\left(\frac{3}{\delta}\right)}}. \tag{8}$$

Along with $(\gamma_l, \gamma_r,$ and $\delta)$, the mean (η) of the AGGD is also computed as follows:

$$\eta = (\vartheta_r - \vartheta_l) \frac{\Gamma\left(\frac{2}{\delta}\right)}{\Gamma\left(\frac{1}{\delta}\right)}. \tag{9}$$

The $(\gamma_l, \gamma_r, \delta, \eta)$ of AGGD are computed on $(\mathbb{C} \in \{D, S, A, A_x, A_y\}; \mathbb{C}$: chromatic maps) across two scales, and the features are averaged over the frames to estimate the overall AGGD feature set (F_{AGGD}) as

$$F_{\text{AGGD}} = \frac{1}{\tau} \sum_{n=1}^{\tau} \left[\gamma_{ln}^{\mathbb{C}q}, \gamma_{rn}^{\mathbb{C}q}, \delta_n^{\mathbb{C}q}, \eta_n^{\mathbb{C}q}\right]. \tag{10}$$

Besides F_{AGGD}, the first three statistical moments, i.e., mean $(\mathcal{M})$, skewness $(\mathcal{S})$ and kurtosis $(\mathcal{K})$ are computed on two chromatic components O_1 and O_2 across two scales. The moment features $(\mathcal{M}_{0_{n1}}, \mathcal{M}_{0_{n2}})$ of O_1 and O_2 are computed on individual frames to estimate the frame level moment feature set as follows:

$$\mathcal{M}_{0_{n1}} = \left[\mathcal{M}\left(O_{n1}^q\right), \mathcal{S}\left(O_{n1}^q\right), \mathcal{K}\left(O_{n1}^q\right)\right] \tag{11}$$

$$\mathcal{M}_{0_{n2}} = \left[\mathcal{M}\left(O_{n2}^q\right), \mathcal{S}\left(O_{n2}^q\right), \mathcal{K}\left(O_{n2}^q\right)\right]. \tag{12}$$

Then, the overall moment features $(\hat{\mathcal{M}})$ of LV is computed by calculating the mean across the frames as follows:

$$\hat{\mathcal{M}} = \frac{1}{\tau} \sum_{n=1}^{\tau} \left[\mathcal{M}_{0_{n1}}, \mathcal{M}_{0_{n2}}\right]. \tag{13}$$

Finally, the overall chromatic quality discernible feature set (F_c) is obtained by concatenating F_{AGGD} and $\hat{\mathcal{M}}$ as follows:

$$F_c = \left[F_{\text{AGGD}}, \hat{\mathcal{M}}\right]. \tag{14}$$

These F_c features are computed at two scales, which results a feature set of size 1×52.

B. Quality Prediction

The overall quality aware feature set (F) of distorted LVs is obtained by concatenating $F_{\text{Gabor}}, F_{\text{LBP}}, F_c$ as follows:

$$F = [F_{\text{Gabor}}, F_{\text{LBP}}, F_c]. \tag{15}$$

In our work, we utilized ABPNN [15] to predict the quality of distorted LVs. The ABPNN model was trained with the cardinality of the input layer set to the size of the feature set F. Two hidden layers were incorporated, each comprising eighty-four neurons. We applied tangent sigmoid and ReLU transfer functions for the first and second hidden layers. A pure linear transfer function was employed for the single-node output layer. The ABPNN model was trained over 50 epochs with an initial learning rate set to 0.001, and the number of base learners was 10. For training, the surgeons opinion scores are normalized into the [0, 1].

III. RESULTS AND DISCUSSIONS

We assess the efficacy of the proposed model on the LVQA dataset [11]. The LVQA database consists of 210 surgical LVs, of which 10 are of pristine quality, and five types of distortions are applied to each pristine LV with four levels each to create 200 distorted LVs. The applied distortions include AWGN, motion blur, defocus blur, smoke, and uneven illumination. The pristine LVs are captured at 25 fps with a 512×288 resolution. Each LV is accompanied by a mean opinion score ranging from 0 to 3, which serves as an expert representative score.

To evaluate the efficacy of the proposed QA for surgical LVs, we randomly partitioned the overall features of the LVQA dataset into two distinct nonoverlapping feature subsets, i.e., training (80%) and testing (20%). This random allocation process is iterated over 500 iterations, and for each random split, we computed Spearman rank order correlation coefficient (SROCC) and linear correlation coefficient (LCC). These metrics gauge the relationship between surgeon opinion scores and the predicted quality scores. Finally, the mean LCC and SROCC scores across 500 iterations are reported. The mathematical descriptions of LCC and SROCC are as follows:

$$\text{LCC} = \frac{\sum_{j=1}^{\mathbb{N}} \left(\rho_j - \overline{\rho}_j\right)\left(\varrho_j - \overline{\varrho}_j\right)}{\sqrt{\sum_j \left(\rho_j - \overline{\rho}_j\right)^2} \sqrt{\sum_j \left(\varrho_j - \overline{\varrho}_j\right)^2}} \tag{16}$$

$$\text{SROCC} = 1 - \frac{6 \sum_{j=1}^{\mathbb{N}} \Delta_j^2}{\mathbb{N}\left(\mathbb{N}^2 - 1\right)} \tag{17}$$

where j ($j = 1, 2 \ldots \mathbb{N}$; $\mathbb{N}$ = total number of LVs) is the sequence of LVs present in the LVQA dataset. In this context, ρ and ϱ represent the predicted and surgeon opinion scores, respectively, and $\overline{\rho}$ and $\overline{\varrho}$ denote the mean values of ρ and ϱ, respectively.

For a fair comparison, we selected three FR video quality assessment (VQA) models (Appina [8], STMAD [4], SPEED [5]), and five supervised NR VQA models (TLVQM [6], Biswas and Palaniswamy [9], VQP-Net [11], VIIDEO [7], and Poreddy et al. [12]). Appina [8] computes the video-level attributes of distorted LVs using various spatial and spectral distance measurements. STMAD [4] evaluates the spatio-temporal attributes of LVs by analyzing the motion disparities between frames. SPEED [5] is an FR IQA model that determines the quality of test LVs by comparing the spatial-entropy information of pristine and distorted LVs. TLVQM [6] computes both low and high-level complex features of LVs by analyzing various motion attributes

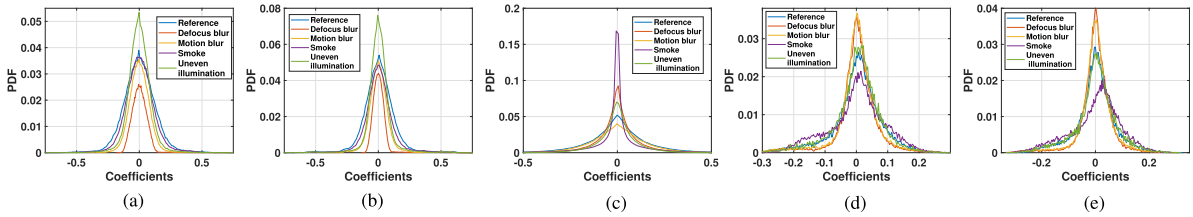

Fig. 3. Histograms of five chromatic maps (D, S, A, A_x, A_y) of 100^{th} frame of reference and distorted versions of 'video 10' of the LVQA dataset.

Table 1. Overall and Distortion Wise LCC Scores of Different VQA Models on the LVQA dataset [11]

Type	Model	AWGN	Defocus blur	Motion blur	Uneven illumination	Smoke	Overall
FR VQA	Appina [8]	0.9987	0.9673	0.9396	0.9473	0.9854	0.9454
	STMAD [4]	0.9585	0.8567	0.9604	0.8565	0.9296	0.7838
	SPEED [5]	0.9461	0.9033	0.9396	0.9501	0.9747	0.6424
NR VQA	TLVQM [6]	0.7651	0.7066	0.7493	0.5986	0.6321	0.6893
	BISWAS [9]	-	-	0.9842	-	-	-
	VQP-Net [11]	-	-	-	-	-	0.8992
	VIIDEO [7]	0.8658	0.5136	0.3498	0.4035	0.4195	0.3744
	Poreddy [12]	**0.9992**	**0.9828**	**0.9803**	0.9624	0.9742	0.9563
	Proposed	0.9986	0.9532	0.9608	**0.9763**	**0.9801**	**0.9800**

Table 2. Overall and Distortion Wise SROCC Scores of Different VQA Models on the LVQA dataset [11]

Type	Model	AWGN	Defocus blur	Motion blur	Uneven illumination	Smoke	Overall
FR VQA	Appina [8]	0.9701	0.9701	0.9461	0.9286	0.9333	0.9309
	STMAD [4]	0.9374	0.9276	0.8245	0.8122	0.9077	0.7780
	SPEED [5]	0.9110	0.9276	0.9136	0.9448	0.9291	0.6357
NR VQA	TLVQM [6]	0.7591	0.7386	0.7031	0.5998	0.6326	0.3334
	VQP-Net [11]	-	-	-	-	-	0.8434
	VIIDEO [7]	0.8822	0.3023	0.3915	0.4281	0.4416	0.3334
	Poreddy [12]	0.9126	0.9252	0.8810	0.8998	0.9232	0.9107
	Proposed	**0.9733**	**0.9419**	**0.9337**	**0.9048**	**0.9540**	**0.9247**

Table 3. LCC Scores of Individual Features on the LVQA dataset [11]

Feature	AWGN	Defocus blur	Motion blur	Uneven illumination	Smoke	Overall
Gabor	0.9724	0.8412	0.9229	0.9201	0.8335	0.8565
Texture	0.9709	0.9842	0.9636	0.5521	0.8503	0.8853
color	0.9601	0.8898	0.8939	0.9067	0.9270	0.9271
Overall	0.9986	0.9532	0.9608	0.9763	0.9801	0.9800

between the frames. Biswas [9] predicts the quality of motion blur LVs using the model parameters of BGGD. VQP-Net [11] calculates the quality score of distorted LVs by employing stacked ResNet-18 architectures. VIIDEO [7], Poreddy [12] are supervised QA models that predicts the quality of a test LV based on the scene statistics of the LV. These supervised models are retrained on the LVQA dataset using the different regressors with the same model parameters and codes released by the respective authors.

Tables 1 and 2 present both the distortion-wise and overall LCC and SROCC scores of the LVQA dataset. The tables clearly demarcate that the proposed model performance scores surpassed those of the compared NR VQA models, indicating superior performance.

Table 3 presents the mean LCC and SROCC scores of the individual proposed features on the LVQA dataset across 500 random train and test splits. The performance scores show that each feature contributed significantly in achieving the best performance scores across all distortion types.

IV. CONCLUSION

This work proposes an opinion-aware QA model based on statistical disparities between luminance and chromatic components of LVs. The proposed model extracts luminance components based on Gabor and LBP features, chromatic attributes from AGGD and moment statistics of the OCS. Further, these features are pooled across the number of LV frames and mapped to the quality score of a test LV using a trained ABPNN. In the future, exploring the statistical features of luminance and chromatic components, along with motion variations, to develop an unsupervised LVQA model will be an exciting area of research.

ACKNOWLEDGMENT

This work was supported in part by the Science and Engineering Research Board (SERB), India, under Grant EEQ/2021/000804, and in part by the Fund for Improvement of Science and Technology Infrastructure (FIST), DST, India, under Grant SR/FST/ET-I/2020/5.

REFERENCES

[1] PR Newswire, "Global laparoscopic devices market to reach 15.8 billion by 2026," 2021. [Online]. Available: https://www.prnewswire.com/news-releases/global-laparoscopic-devices-market-to-reach-15-8-billion-by-2026--301323890.html

[2] A. Faragasso, S. Mitchel, S. Cosentino, and H. Asama, "Toward multicamera systems for minimally invasive surgery," *IEEE Sens. Lett.*, vol. 7, no. 3, Mar. 2023, Art. no. 6001304.

[3] Z. A. Khan and A. Beghdadi, "Towards a video quality assessment based framework for enhancement of laparoscopic videos," *Proc. SPIE*, vol. 11316, pp. 129–136, 2020.

[4] P. V. Vu, C. T. Vu, and D. M. Chandler, "A spatiotemporal most-apparent-distortion model for video quality assessment," in *Proc. 18th Int. Conf. Image Process.*, 2011, pp. 2505–2508.

[5] C. G. Bampis, P. Gupta, R. Soundararajan, and A. C. Bovik, "SpEED-QA: Spatial efficient entropic differencing for image and video quality," *IEEE Signal Process. Lett.*, vol. 24, no. 9, pp. 1333–1337, Sep. 2017.

[6] J. Korhonen, "Two-level approach for no-reference consumer video quality assessment," *IEEE Trans. Image Process.*, vol. 28, no. 12, pp. 5923–5938, Dec. 2019.

[7] A. Mittal, M. A. Saad, and A. C. Bovik, "A completely blind video integrity oracle," *IEEE Trans. Image Process.*, vol. 25, no. 1, pp. 289–300, Jan. 2016.

[8] H. H. Borate, P. A. Kara, B. Appina, and A. Simon, "A full-reference laparoscopic video quality assessment algorithm," *Opt. Photon. Inf. Process. XV*, vol. 11841, pp. 55–61, 2021.

[9] S. Biswas and R. Palanisamy, "Quality evaluation of laparoscopic videos using the interdependency of luminance and texture maps," in *Proc. Int. Conf. Signal Process. Integr. Netw.*, 2023, pp. 103–108.

[10] T.-S. Nguyen, J. Chaussard, M. Luong, H. Zaag, and A. Beghdadi, "A no-reference measure for uneven illumination assessment on laparoscopic images," in *Proc. Int. Conf. Image Process.*, 2022, pp. 4103–4107.

[11] Z. A. Khan, A. Beghdadi, M. Kaaniche, F. Alaya-Cheikh, and O. Gharbi, "A neural network based framework for effective laparoscopic video quality assessment," *Computerized Med. Imag. Graph.*, vol. 101, 2022, Art. no. 102121.

[12] A. K. R. Poreddy, B. V. Atmakuru, T. B. Krishna, P. Kokil, and B. Appina, "Enhancing laparoscopic video quality assessment: A model addressing sensor and channel distortions," *IEEE Sens. Lett.*, vol. 8, no. 3, Mar. 2024, Art. no. 6003104.

[13] D. J. Field, "Relations between the statistics of natural images and the response properties of cortical cells," *J. Opt. Soc. Amer. A*, vol. 4, no. 12, pp. 2379–2394, 1987.

[14] T. Ojala, M. Pietikainen, and T. Maenpaa, "Multiresolution gray-scale and rotation invariant texture classification with local binary patterns," *IEEE Trans. Pattern Anal. Mach. Intell.*, vol. 24, no. 7, pp. 971–987, Jul. 2002.

[15] P. Bartlett and M. Traskin, "Adaboost is consistent," in *Adv. Neural Inf. Process. Syst.*, vol. 19, 2006, pp. 105–112.